Quadrupole scattering in $PrAl_2$

M. J. Sablik
Southwest Research Institute, San Antonio, Texas 78284

P. Pureur, G. Creuzet, and A. Fert
Laboratoire de Physique des Solides, Université de Paris—Sud, F-91405 Orsay, France

P. M. Levy
Department of Physics, New York University, 4 Washington Place, New York, New York 10003
(Received 28 March 1983)

We derive the spontaneous anisotropy of the resistivity of the ferromagnetic compound $PrAl_2$ from magnetoresistance measurements on a single crystal of $PrAl_2$. We ascribe this spontaneous anisotropy of the resistivity to scattering of the conduction electrons by the thermal quadrupole disorder and we account for our experimental results by using the theoretical model previously developed by us. We find that quadrupole scattering gives a very important contribution to the total magnetic disorder (spin and quadrupole) resistivity but that only a small part of this quadrupole contribution is anisotropic.

I. INTRODUCTION

The $4f$ electrons of rare-earth ions with $L \neq 0$ carry not only a spin but also a quadrupole moment. This gives rise, in metallic systems, to quadrupole scattering of the conduction electron in addition to the conventional spin scattering.

The anisotropic resistivity arising from quadrupole scattering is well known in metals containing rare-earth impurities.[1–6] Here anisotropic means different according to whether the quadrupole axes are parallel or perpendicular to the current direction. This anisotropic resistivity of dilute alloys can be easily investigated by magnetoresistance measurements: One polarizes the rare-earth impurities by an applied magnetic field parallel and then perpendicular to the current; the difference between the resistivities is related in a straightforward manner to the qaudrupole scattering. This type of measurement has been used to determine the quadrupole term of the $4f$-conduction-electron interaction. It has been found that, in some systems, the quadrupole term is as large or larger than the spin-exchange term.[1,4,6]

The problem of quadrupole scattering is somewhat different in the case of rare-earth intermetallic compounds. Consider the case of a ferromagnetic compound. For $T \ll T_c$ the spins and the quadrupole are perfectly aligned. The spin and quadrupole potentials are periodic and there is no spin or quadrupole scattering. Nevertheless, as the temperature is increased, thermal disorder gives rise to spin- and quadrupole-disorder scatterings. Previously, we showed that quadrupole-disorder scattering in a ferromagnetic compound results in a spontaneous anisotropy of the resistivity, the resistivity being different according to whether the spontaneous magnetization is parallel or perpendicular to the current. However, the spontaneous anisotropy of ferromagnetic compounds is expected to be smaller than the induced anisotropy in dilute alloys for the following reason. Rare-earth impurities in alloys generally have a strong spin-independent scattering potential. There exist interference terms between potential and quadrupole scatterings, which give relatively large and strongly anisotropic resistivity terms. For example, in a noble metal with rare-earth impurities, the anisotropic part of the magnetoresistance due to quadrupole scattering is definitely larger than the isotropic part due to exchange scattering.[1] In contrast, for intermetallic compounds, there is no potential scattering (the spin-independent potential is periodic) and the resistivity terms previously calculated by us[7] come from taking the quadrupole interaction to second order. This gives rise to a quadrupole resistivity term which includes an isotropic part much larger than the anisotropic part.

These differences predicted between the problem of quadrupole scattering in alloys and compounds led us to investigate the spontaneous anisotropy of the resistivity (SAR) of the ferromagnetic compound $PrAl_2$. As a matter of fact, Christen[8] was the first to observe a SAR in $PrAl_2$ and $DyAl_2$ compounds. However, while the evidence of SAR is quite clear in the experimental results of Christen, we questioned the method used to extract values of the SAR from the magnetoresistance curves. Thus, we performed new magnetoresistance measurements on a piece of the single crystal of $PrAl_2$ used in Christen's previous measurements. In this paper, we present the experimental results together with an analysis of the data, and we compare our results with predictions based on the theoretical model we previously developed and have now adapted to $PrAl_2$.

II. EXPERIMENTAL TECHNIQUES

We measured the magnetoresistance properties of a single crystal of $PrAl_2$ which was provided to us by Dr. M. Christen and Professor J. Sierro of Université de Genève. The crystal-growth method has been described in a previous work.[9,10] The sample obtained by spark cutting was a slab ($9 \times 1.5 \times 0.6$ mm) with face orientations as indicated on Fig. 1. The resistivity was measured by a conventional

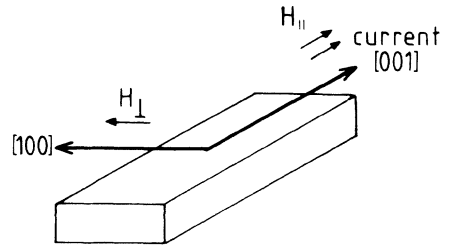

FIG. 1. Sample geometry. The current direction, the longitudinal and transverse field orientations, and the crystal axes are indicated.

ac technique in the magnetic field of a superconducting coil (up to 25 kG) and for temperatures between 4.2 and 35 K. By rotating the sample the magnetic field could be applied along the current direction or perpendicular to it (in the plane of the slab). As indicated in Fig. 1, both directions of the field correspond to equivalent easy axes of the magnetization [001] and [100]. The magnetoresistance curves were generally recorded by decreasing the field from its maximum value.

III. EXPERIMENTAL RESULTS

The temperature dependence of the zero-field resistivity of $PrAl_2$ is shown in Fig. 2. To derive the contribution to the resistivity from magnetic disorder, we subtracted the residual resistivity and the phonon resistivity of $PrAl_2$ which to a good approximation can be taken as the resistivity of $LaAl_2$.[11] In this way, we obtained the magnetic disorder resistivity shown in Fig. 3.

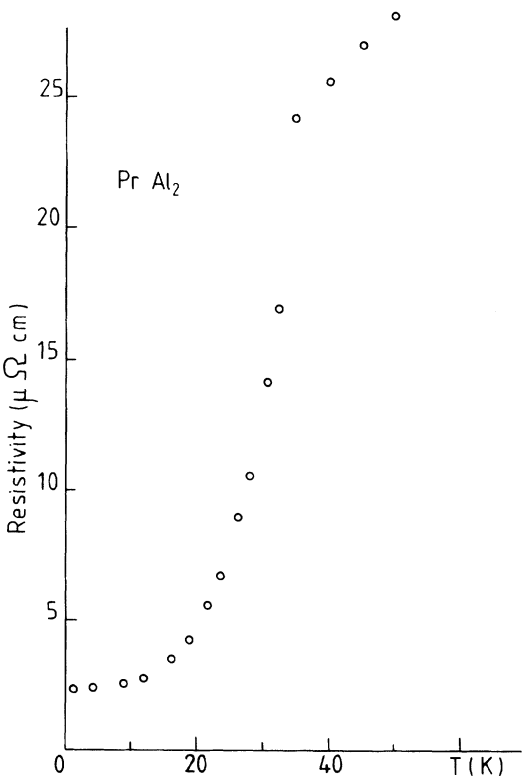

FIG. 2. Zero-field resistivity of our $PrAl_2$ sample.

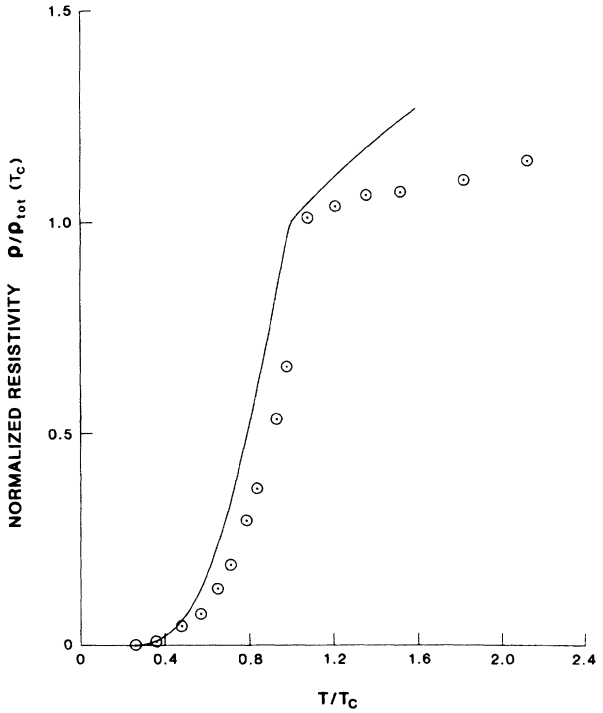

FIG. 3. Resistivity as a function of temperature in $PrAl_2$. All points are normalized relative to $\rho(T=T_c)$. Circled points represent experimental values and the solid curve is the theoretical fit. Absence of correlation effects in the theoretical calculations is believed to account for the difference between theory and experiment.

Typical examples of magnetoresistance curves are shown in Fig. 4. First we discuss the results at low temperatures [see Fig. 4(a)]. For $T \ll T_c$ the variation of the resistivity as a function of the applied field, which is called magnetoresistance, has two origins: (1) when the domains are reoriented we obtain a contribution from the spontaneous anisotropy of the resistivity (SAR), and (2)

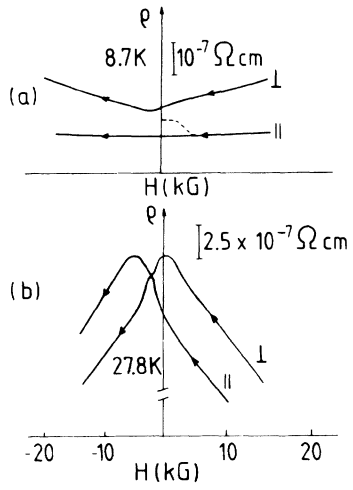

FIG. 4. Two examples of experimental magnetoresistance curves in decreasing fields from 22 to −22 kG, at (a) 8.7 K and at (b) 27.6 K. The dashed line in Fig. 4(a) represents the first magnetization curve in longitudinal fields.

the normal magnetoresistance, i.e., that due to the Lorentz force. The low-field range is rather difficult to analyze because the SAR contribution changes during reorientations of the domains. (In particular, the asymmetry between the behavior at positive and negative fields is due to remanence effects.) In contrast, the quasilinear (and symmetric) variation observed at higher fields corresponds to a simple situation in which the sample is monodomain. Then the contribution from the SAR to the splitting between the longitudinal and transverse curves is saturated and the linear variation of the resistivity is due only to normal magnetoresistance (which is larger in transverse fields as usual). As it is well known, normal magnetoresistance obeys the Kohler rule, which, in ferromagnets, can be written as[12]

$$\frac{\Delta\rho_N^{\parallel}}{\rho_0^{\parallel}}=K_{\parallel}\left[\frac{B}{\rho_0}\right], \qquad \frac{\Delta\rho_N^{\perp}}{\rho_0^{\perp}}=K_{\perp}\left[\frac{B}{\rho_0}\right], \tag{1}$$

where $\rho_0^{\parallel}(\rho_0^{\perp})$ is the resistivity for zero induction ($B=0$) when the magnetization is longitudinal (transverse) and B is the magnetic induction [$B=H+4\pi(1-D)$, where D is the demagnetization factor, which is different for the longitudinal and transverse fields applied to our sample.] In principle, this normal magnetoresistance can be subtracted if the Kohler functions $K_{\parallel}$ and $K_{\perp}$ are known. However, a simple and conventional method consists in extrapolating the high-field linear variation down to zero induction $B=0$, i.e., to $H_0^{\parallel}=-4\pi M(1-D_{\parallel})$ for the longitudinal curves and $H_0^{\perp}=-4\pi M(1-D_{\perp})$ for the transverse curves, as shown schematically in Fig. 5. This method overlooks the fact that the function $K(B/\rho_0)$ becomes quadratic at very small values of B/ρ_0. According to what we know about the Kohler functions from measurements on $PrAl_2$ at high temperature, the resulting error is negligible; therefore we adopted this extrapolation method. The demagnetization factors were derived from numerical calculations by Osborn,[13] and the magnetization values were obtained from the experimental results of Purwins *et al.*[14] In Fig. 6 we present some examples of extrapolation showing the extrapolated values $\rho_{\parallel}^{\text{extpl}}(B=0)$ and $\rho_{\perp}^{\text{extpl}}(B=0)$. We indicate by arrows the fields $H_0^{\parallel}$ and $H_0^{\perp}$ which give $B=0$. The spontaneous anisotropy of the resistivity ($\rho_{\parallel}-\rho_{\perp}$) in our notation is given by

$$\rho_{\parallel}-\rho_{\perp}=\rho_{\parallel}^{\text{extpl}}(B=0)-\rho_{\perp}^{\text{extpl}}(B=0)\ . \tag{2}$$

As the temperature is raised a negative magnetoresistance associated with the induced magnetization term (i.e., due to the reduction of the magnetic disorder in the presence of a field) becomes more and more important (Fig. 5). The slopes in high fields become negative above about 16 K [see Figs. 4(b) and 6]. This negative contribution appears to be linear and is nearly isotropic, as can be seen by comparing the slopes of the longitudinal and transverse curves in the temperature range where the negative term predominates. This means that, for the same *internal* field, the negative contribution is the same for longitudinal and transverse orientations. As the internal fields for $H=H_0^{\parallel}$ and $H=H_0^{\perp}$ are equal ($H_{\text{in}}\equiv H-4\pi DM=-4\pi M$ for $H=H_0^{\parallel}$ and $H=H_0^{\perp}$), the contributions to $\rho_{\parallel}^{\text{extpl}}(B=0)$ and $\rho_{\perp}^{\text{extpl}}(B=0)$ are equal and do not contribute to their difference $\rho_{\parallel}^{\text{extpl}}(B=0)-\rho_{\perp}^{\text{extpl}}(B=0)$. Thus, Eq. (2) remains valid and can still be used to derive $\rho_{\parallel}-\rho_{\perp}$ at $T\lesssim T_c$. Figure 6 shows some examples of the determination of $\rho_{\parallel}-\rho_{\perp}$ in this range. We emphasize that this method allows us to single out the SAR easily. In contrast, Christen[8] considers the difference between $\rho_{\parallel}$ and $\rho_{\perp}$ at fields corresponding to different values of B and likely mixes contributions from normal magnetoresistance and spin-exchange scattering to the SAR.

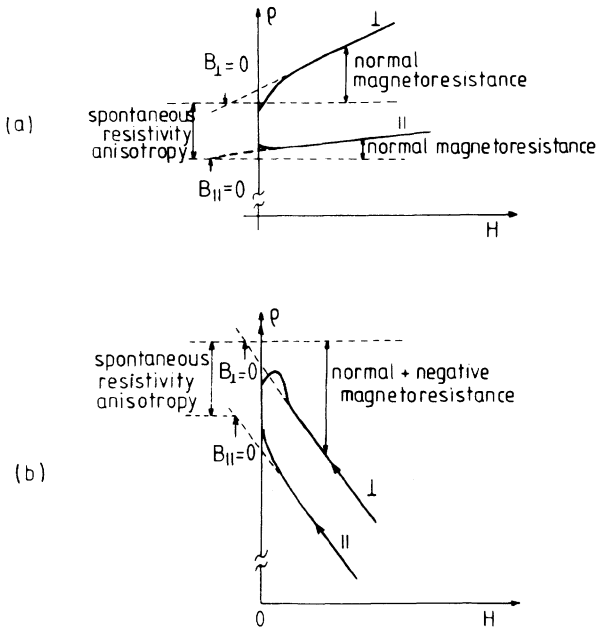

FIG. 5. Scheme showing the different contributions to the magnetoresistance (a) with spontaneous anisotropy of the resistivity and normal magnetoresistance; (b) in addition, with the negative contribution due to the reduction of the magnetic scattering by applied fields.

We obtained in this way the spontaneous anisotropy of the resistivity shown in Fig. 7. The gross features of the temperature dependence correspond to what is expected by our previous calculations,[7] the SAR increasing to a maximum value at a temperature slightly below T_c and then decreasing to zero at T_c. However, at low temperatures, $\rho_{\parallel}-\rho_{\perp}$ does not decrease to zero which means that for the anisotropic part of the resistivity, Fig. 7, as well as for the total resistivity, Fig. 2, there is a residual contribution due to impurity and defect scattering in addition to the thermal contribution. As we are not interested in the anisotropy of the residual scattering, we subtract its contribution by assuming that it varies between $T=0$ and $T=T_c$ as the spontaneous magnetization of $PrAl_2$. The dashed line in Fig. 7 shows this variation. After subtracting this term from the experimental points, we obtain Fig. 8. As we do not know the origin of this residual scattering, our assumption that its contribution to the SAR is proportional to the spontaneous magnetization is questionable. We have tried the alternative assumption that it

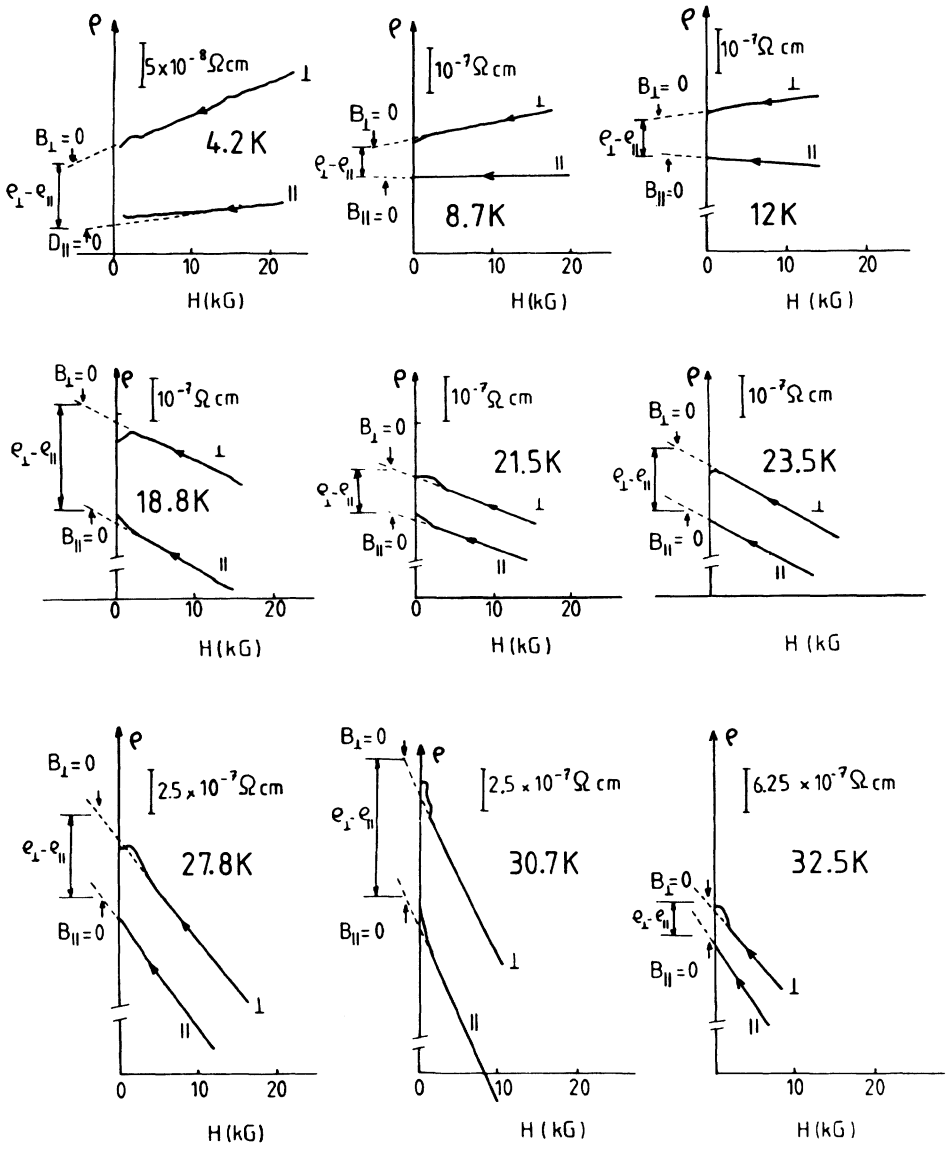

FIG. 6. Determination of the spontaneous anisotropy of the resistivity from experimental data at several temperatures.

varies as the square of the spontaneous magnetization; however, this does not significantly alter the results of Fig. 8.

IV. MODEL CALCULATION AND DISCUSSION

The theoretical model[7] we use to interpret the resistivity data uses transport theory described by Ziman[15] and the assumption of single-ion scattering. The spin- and quadrupole-disorder contributions to the resistivity are given as[7]

$$\rho_{ex}=3K_1(\tfrac{6}{7})^2R_3^{ex}(0,0)^2(g_J-1)^2$$

$$\times[\langle O^1_{-1}O^1_1\rangle_w+\langle O^1_1O^1_{-1}\rangle_w]\,, \tag{3a}$$

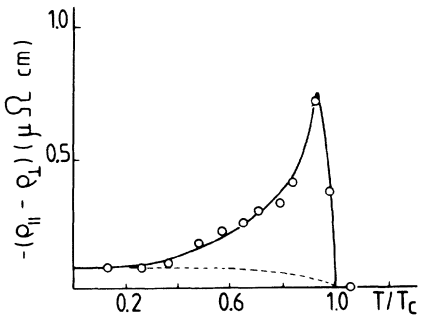

FIG. 7. Spontaneous anisotropy of the resistivity vs temperature T/T_c ($T_c=33$ K). The solid line is a guide for the eye. The dashed line represents the contribution from residual scattering when this contribution is assumed to be proportional to the magnetization. Magnetization data were taken from Ref. 14.

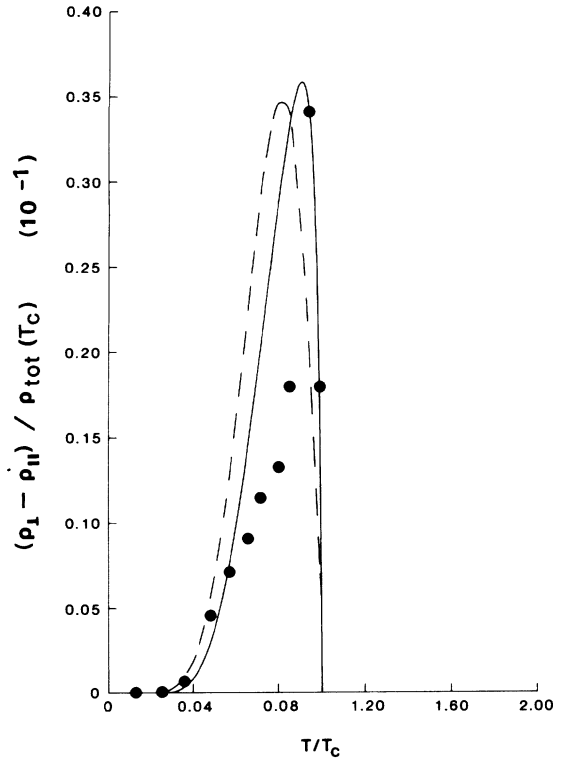

FIG. 8. Dependence of resistivity difference $\rho_{\perp}-\rho_{||}$ on temperature in $PrAl_2$. The circles show the experimental values divided by the value of the "magnetic" contribution to the resistivity at the Curie temperature. The solid curve shows the similarly normalized theoretical fit. For this fit, we used $\lambda_1=-5.87$ K, $\lambda_2=-0.01$ K, and conduction-electron partial-wave weights of $\alpha_0=0.8$, $\alpha_1=0.6$, $\alpha_2=0.6$, and $\alpha_3=2.0$. The dashed curve is for $\lambda_2=0$.

$$\rho_q^{||}=K_1\langle r^2\rangle^2\left[\frac{2^3\times3^4\times7}{4^2\times5^5}\right]n_0^2F_q(J,S,L)\times\sum_Q(-1)^Q[\langle O^2_{-Q}O^2_Q\rangle_w-\langle O^2_{-Q}\rangle\langle O^2_Q\rangle]I_Q\ , \tag{3b}$$

where $\langle AB\rangle_w$ is the weighted thermal average,

$$\langle AB\rangle_W=\frac{1}{Z}\sum_{\gamma,\gamma_0}e^{-E_{\gamma_0}/k_BT}\left[\frac{(E_{\gamma_0}-E_\gamma)/k_BT}{1-e^{-(E_{\gamma_0}-E_\gamma)/k_BT}}\right]\times\langle\gamma_0|A|\gamma\rangle\langle\gamma|B|\gamma_0\rangle\ . \tag{4}$$

Here $|\gamma\rangle$ is a crystal-field state modified by the presence of a molecular field, $Z=\sum_\gamma\exp(-E_\gamma/k_BT)$ is the partition function for the states $|\gamma\rangle$, n_0 is the number of electron or holes (whichever is less) in the $4f$ shell, $F_q(J,S,L)$ is a dimensionless combination of 6-j and fractional-parentage coefficients, $O^1_{\pm1}$ and O^2_Q are spherical tensor operators of ranks 1 and 2, $\langle r^2\rangle$ is the mean-square radius of the $4f$ shell, g_J is the Lande g factor, and $R_3^{ex}(0,0)$ is a radial exchange integral.

To obtain $\rho_q^{\perp}$, we note that the tensor operators O^2_Q are quantized along the current direction whereas the states $|\gamma\rangle$ and $|\gamma_0\rangle$ are quantized along the direction of the spontaneous magnetization. Thus, if the current is perpendicular to the magnetization, the O^2_Q operators must be rotated into the ordering direction before they can operate on states $|\gamma\rangle$ and $|\gamma_0\rangle$. To carry out the calculation of $\rho_q^{\perp}$, we use the well-known rotation relation[16]

$$O^2_Q=\sum_{Q'}d^2_{Q'Q}(\pi/2)O^2_{Q'}\ , \tag{5}$$

where the $d^2_{Q'Q}(\pi/2)$ are rotation coefficients, and then evaluate the matrix elements of $O^2_{Q'}$ entering Eq. (3b).

In our previous formulation, conduction electrons were treated as plane waves decomposed into a set of partial waves, with only s waves contributing significantly to exchange scattering. Higher-order partial waves contribute to quadrupole scattering, and the effects of these partial-wave scatterings are lumped into the constants I_Q, which consist of complicated combinations of $3j$ coefficients and radial integrals.

One feature not predicted by our previous model calculations[7] is the proper sign of the anisotropy. To rectify this in our present formulation, we consider our conduction electrons as plane waves admixed with the open-shell electrons from the rare earth, e.g., $5d$, and with an enhanced f-wave component due to orthogonalization to the $4f$ core states. While the form of these radial integrals should in some measure reflect the admixed atomic radial functions, we will for simplicity assume that the radial wave functions for the conduction electrons are given by spherical Bessel functions. Then the radial integrals entering Eq. (3b) via I_P take the form

$$R^c_h(s,t)=\alpha_s\alpha_t\int_0^\infty\int_0^\infty j_s(k_Fr_2)j_t(k_Fr_2)\frac{r_<^h}{r_>^{h+1}}\times|P_{nl}(r_1)|^2r_1^2r_2^2dr_1dr_2\ , \tag{6}$$

where

$$\frac{r_<^h}{r_>^{h+1}}=\begin{cases}r_1^h/r_2^{h+1}, & \text{if } r_2>r_1\\ r_2^h/r_1^{h+1}, & \text{if } r_1>r_2\end{cases}. \tag{7}$$

The function $j_s(x)$ is a spherical Bessel function or order s, and $P_{nl}(x)$ is a $4f$ hydrogenic wave function.[17] The expression (6) differs from the radial integrals used in our previous model in that the sth and tth partial waves from the plane-wave expansion at the Fermi surface are now weighted by factors α_s and α_t, which are numbers of the order of 1. A similar weighting appears in $R_3^{ex}(0,0)$ in Eq. (3a). Thus *our conduction electrons are no longer plane waves.*

The molecular-field (MF) states $|\alpha\rangle$ for $PrAl_2$ are obtained from the Hamiltonian,

$$H_{MF}=\sum_i\{B_4[O_0^4(i)+5O_4^4(i)]+B_6[O_0^6(i)-21O_4^6(i)]+\lambda_1\langle O_0^1\rangle O_0^1(i)+\lambda_2\langle O_0^2\rangle O_0^2(i)\}\ , \tag{8}$$

with $B_4=-38.5\times10^{-4}$ meV and $B_6=-54.7\times10^{-6}$ meV, which corresponds to $x=0.77$ and $W=-0.30$ meV found from the inelastic neutron scattering studies of Purwins *et al.*[18] If we fit to a Curie temperature of 33 K, we find $\lambda_1=-136.5$ kG/μ_B, which yields a zero-

temperature moment at the Pr site of $3.10\mu_B$. Polarized neutron scattering[19] and hyperfine-field[20] investigations indicate that the conduction-electron polarization[21] present in the first half of the RAl_2 series, where R represents rare earth, opposes the localized $4f$ moment; therefore, it is reasonable that this polarization reduces the measured moment to $2.94\mu_B$.[14] As indicated by the form of Eq. (8), ordering is taken to be in the $\langle 001 \rangle$ direction. The biquadratic term in Eq. (8) is included because it is needed to fit the anisotropy in the resistivity, as seen below. The Fermi wave vector for $PrAl_2$ is taken to be 0.62 Å^{-1}. The normalized values obtained for the resistivity (see Fig. 3), however, are not very sensitive to changes in this value.

To produce a negative result for $\rho_{||}-\rho_{\perp}$, it is necessary to increase the weight of the f-partial-wave contribution at the Fermi surface. Figure 8 shows our fit to the experimental data for a partial-wave weighting of $\alpha_0=0.8$, $\alpha_1=0.6$, $\alpha_2=0.6$, and $\alpha_3=2.0$, corresponding to s, p, d, and f waves, respectively. The dashed curve in Fig. 8 is for $\lambda_2=0$ whereas the solid curve is for $\lambda_2=-0.01$ K. While the weightings α_0, α_1, α_2, and α_3 influence the magnitude of the anisotropy, it appears that the strength of the biquadratic coupling adjusts the location of the peak in $\rho_{\perp}-\rho_{||}$ as a function of temperature.

As an independent test of our result, we show the functional dependence of magnetization on temperature in Fig. 9. With $\lambda_2=-0.01$ K, the experimental results[14] for the magnetization are in almost direct proportion to the theoretical results, as would be expected to be the case when conduction-electron polarization is taken into account. With $\lambda_2=0$, the functional dependence of the magnetization is not as well reproduced as with $\lambda_2\neq 0$. With $\lambda_2=-0.01$ K, the zero-temperature moment changes almost imperceptibly to $3.12\mu_B$, so that a more sensitive measurement of λ_2 is the fit to the resistance anisotropy (see Fig. 8).

The assertion of substantial f-wave contribution to the conduction electrons at the Fermi surface finds support in the band-structure predictions of Switendick[22] and Hasegawa and Yanase,[23] who analyzed the electronic structure of $LaAl_2$ and YAl_2. Further support for considerable f admixture at the Fermi surface may be seen in the de Haas–van Alphen work of Seitz *et al.*[24]

In Fig. 3 we present our fit to the *total* resistivity as a function of temperature. In Fig. 10 we show that quadrupole scattering ρ_q makes an overwhelmingly dominant contribution to the total resistivity ρ of $PrAl_2$. According to our results, ρ_q is roughly 94% of the total resistivity. It is conceivable that with fewer approximations in the model calculation one might arrive at a lower percentage. On the other hand, this large percentage is not entirely unreasonable for the following reasons. The large quadrupole scattering is firstly indigenous to trivalent praseodymium compounds owing to the large orbital angular momentum $L=5$ compared to the spin $S=1$. This is in-

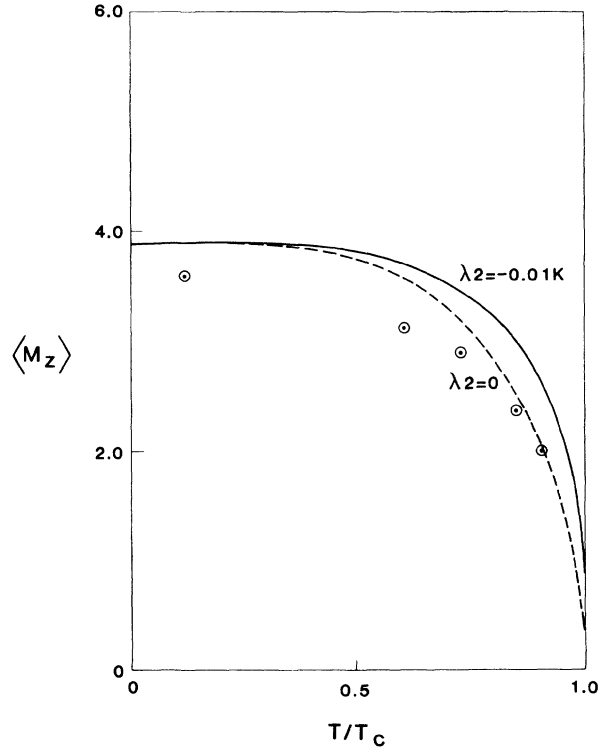

FIG. 9. Magnetization in $PrAl_2$. The circled points are experimental determinations of magnetization per ion (see Ref. 14). The solid curves are theoretical results for the case $\lambda_1=-5.87$ K, $\lambda_2=-0.01$ K. For this case, the magnetization $\langle M_z \rangle$ is in almost direction proportion to the experimental points, the difference being made up by the conduction-electron polarization. The fit is not so good for $\lambda_2=0$ (dashed curve).

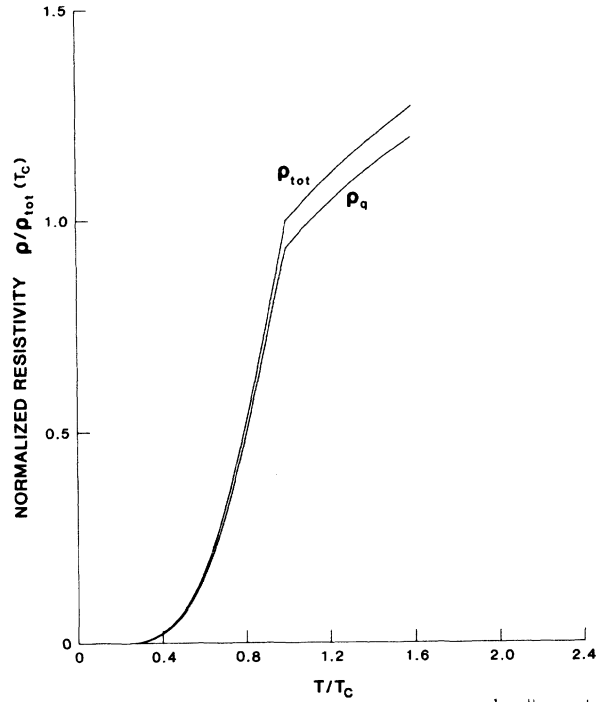

FIG. 10. Quadrupole scattering contribution $\rho_q=\frac{1}{3}(\rho_q^{||}+2\rho_q^{\perp})$ to the total resistivity $\rho_{\text{tot}}=\frac{1}{3}(\rho_{\text{tot}}^{||}+2\rho_{\text{tot}}^{\perp})$. The parameters used to obtain these curves are $B_4=-38.5\times10^{-4}$ meV, $B_6=-54.7\times10^{-6}$ meV, $\lambda_1=-5.87$ K, $\lambda_2=-0.01$ K, and the conduction-electron's partial-wave weights are $\alpha_0=0.8$, $\alpha_1=0.6$, $\alpha_2=0.6$, and $\alpha_3=2.0$. The resistivities are normalized by dividing by the value of ρ_{tot} at $T=T_c=33$ K.

corporated in our formula for the resistivity Eq. (3b) in the factor $F_q(J,S,L)/(g_J-1)^2$, where $F_q(J,S,L)$ is related to the Stevens factor. Secondly, in $PrAl_2$, the quadrupole scattering contribution is particularly dominant because exchange scattering is short ranged and is large only for conduction electrons of small impact parameter (*s* waves), and, according to our results, the *s* component of the conduction electrons near the Fermi surface is suppressed relative to the higher orbital components.

In spite of this large quadrupole contribution to the total (isotropic) scattering, quadrupole scattering does not produce much spontaneous *anisotropy* of the resistivity in $PrAl_2$, i.e., of the order of 3% (see Fig. 8). The reason is that the contribution from quadrupole scattering to the resistivity in compounds comes from the *product* of quadrupole scattering, i.e., from the fluctuations in the aspherical change distribution of the rare-earth ions. This product, see Eq. (3b), contains isotropic terms $I\sum_Q[(-1)^Q \times\langle Q^2_{-Q}O^2_Q\rangle-\langle O^2_{-Q}\rangle\langle O^2_Q\rangle]$, when $I_Q=I$, as well as anisotropic terms when the I_Q are different. In our fits to $PrAl_2$ we find that the I_Q are nearly equal (viz., $I_2:I_1:I_0=1.19:1.0:0.93$). Therefore the isotropic part of the resistivity resulting from quadrupole scattering dominates. As mentioned earlier, this behavior differs markedly from the situation of rare-earth impurities in metals where in an external magnetic field, interference terms between potential and quadrupole scatterings give rise to a relatively large anisotropy in the contribution of rare-earth ions to the resistivity.[1]

Finally, as seen in Fig. 3, the fit to experimental results is not perfect. We have normalized the experimental and theoretical resistivities relative to their values at the Curie temperature. Below T_c, the experimental data rise more sharply as one approaches the Curie temperature than the theoretical results. This can be explained by remembering that the actual resistivity has contributions from short-range correlations, neglected in our mean-field approach.[25] This can account for the sharp rise seen in the experimental curve near T_c. Above T_c the contributions from short-range correlations to the resistivity fall off as temperature increases. The effect of the contributions *diminish* the rise coming from single-ion scattering, as given by our theoretical fit. Therefore short-range correlation effects are able to explain the discrepancies between the experimental resistivity and that predicted on the basis of our mean-field approach.

ACKNOWLEDGMENTS

We thank Professor J. Sierro and Dr. M. Christen for providing us with a single crystal of $PrAl_2$. Also, we acknowledge very helpful discussions with Dr. M. Christen. This work was supported in part by the Centre National de la Recherche Scientifique, France, and the National Science Foundation under Grant No. DMR-81-20673. One of us (P.P.) was supported by the Conselho National de Desenvolvimento Científico Technológico, Brasil.

[1] A. Fert, R. Asomoza, D. H. Sanchez, D. Spanjaard, and A. Friederich, Phys. Rev. B 16, 5040 (1977).
[2] T. Bijvoet, G. Merlijn, and P. Fring, J. Phys. (Paris) Colloq. 39, C5-38 (1978).
[3] R. Asomoza, G. Creuzet, A. Fert, and R. Reich, Solid State Commun. 18, 190 (1978).
[4] J. C. Ousset, G. Carrere, J. P. Vlinet, S. Asbenazy, G. Creuzet, and A. Fert, J. Magn. Magn. Mater. 24, 7 (1981).
[5] G. Lacueva, P. M. Levy, G. Creuzet, A. Fert, and J. C. Ousset, Solid State Commun. 38, 551 (1981).
[6] G. Lacueva, P. M. Levy, and A. Fert, Phys. Rev. B 26, 1099 (1982).
[7] M. Sablik and P. M. Levy, J. Appl. Phys. 49, 2171 (1978).
[8] M. Christen, Solid State Commun. 36, 571 (1980).
[9] M. Christen, B. Giovannini, and J. Sierro, Phys. Rev. B 20, 4624 (1974).
[10] M. Christen, thesis, Genève, 1978 (unpublished).
[11] H. T. van Daal and K. H. J. Buschow, Solid State Commun. 7, 217 (1969).
[12] F. C. Schwerer and J. Silcox, Phys. Rev. Lett. 20, 101 (1968); J. Appl. Phys. 39, 2047 (1968).
[13] J. A. Osborn, Phys. Rev. 67, 351 (1945).
[14] H. G. Purwins, E. Walker, B. Barbara, M. F. Rossignol, and P. Bak, J. Phys. C 7, 3573 (1974).
[15] J. M. Ziman, *Electrons and Phonons* (Oxford University Press, London, 1972), pp. 275–283.
[16] A. R. Edwards, *Theory of Angular Momentum* (Princeton University Press, Princeton, New Jersey, 1957), p. 129.
[17] T. Kaplan and D. H. Lyons, Phys. Rev. 129, 2072 (1963).
[18] H. G. Purwins, W. J. L. Buyers, T. M. Holden, and E. C. Svensson, in *Magnetism and Magnetic Materials, Philadelphia, 1975,* Proceedings of the 21st Annual Conference on Magnetism and Magnetic Materials, edited by J. J. Becker, G. H. Lander, and J. J. Rhyne (AIP, New York, 1976), p. 259.
[19] J. X. Boucherle, D. Givord, A. Gregory, and J. Schweizer, J. Appl. Phys. 53, 1950 (1982).
[20] Y. Berthier, R. A. B. Devine, and E. Belorizky, Phys. Rev. B 17, 4137 (1978).
[21] E. Belorizky, J. J. Niez, and P. M. Levy, Phys. Rev. B 23, 3360 (1981)
[22] A. C. Switendick, Proceedings of the 10th Rare Earth Conference, Carefree, Arizona, 1973, Vol. I, p. 235.
[23] A. Hasegawa and Y. Yanase, J. Phys. F 10, 847 (1980); 10, 2207 (1980).
[24] E. Seitz, B. Lengeler, G. Kamm, and J. Kopp, J. Phys. (Paris) Colloq. 40, C5-76 (1979).
[25] P. G. de Gennes and J. Friedel, J. Phys. Chem. Solids 4, 71 (1958).